



## Biochar alters hydraulic conductivity and impacts nutrient leaching in two agricultural soils

Danielle L. Gelardi<sup>1,2</sup>, Irfan H. Ainuddin<sup>3</sup>, Devin A. Rippner<sup>4</sup>, Janis E. Patiño<sup>5</sup>, Majdi Abou Najm<sup>1</sup>, and Sanjai J. Parikh<sup>1</sup>

<sup>1</sup>Land, Air and Water Resources, University of California, Davis, 1 Shields Ave, Davis, CA 95616, USA

<sup>2</sup>Natural Resources Assessment Section, Washington State Department of Agriculture, Olympia, WA 98504, USA

<sup>3</sup>College of Agriculture, California State University Chico, 400 West First Street, Chico, CA 95929, USA

<sup>4</sup>United States Department of Agriculture, Horticulture Crops Research Unit, Prosser, WA 99350, USA

<sup>5</sup>Department of Civil and Environmental Engineering, University of California, Davis, 1 Shields Ave, Davis, CA 95616, USA

**Correspondence:** Danielle L. Gelardi (dlgelardi@ucdavis.edu)

Received: 19 May 2021 – Discussion started: 27 May 2021

Revised: 4 November 2021 – Accepted: 9 November 2021 – Published: 21 December 2021

**Abstract.** Biochar is purported to provide agricultural benefits when added to the soil, through changes in saturated hydraulic conductivity ( $K_{\text{sat}}$ ) and increased nutrient retention through chemical or physical means. Despite increased interest and investigation, there remains uncertainty regarding the ability of biochar to deliver these agronomic benefits due to differences in biochar feedstock, production method, production temperature, and soil texture. In this project, a suite of experiments was carried out using biochars of diverse feedstocks and production temperatures, in order to determine the biochar parameters which may optimize agricultural benefits. Sorption experiments were performed with seven distinct biochars to determine sorption efficiencies for ammonium and nitrate. Only one biochar effectively retained nitrate, while all biochars bound ammonium. The three biochars with the highest binding capacities (produced from almond shell at 500 and 800 °C (AS500 and AS800) and softwood at 500 °C (SW500)) were chosen for column experiments. Biochars were amended to a sandy loam and a silt loam at 0 % and 2 % ( $w/w$ ), and  $K_{\text{sat}}$  was measured. Biochars reduced  $K_{\text{sat}}$  in both soils by 64 %–80 %, with the exception of AS800, which increased  $K_{\text{sat}}$  by 98 % in the silt loam. Breakthrough curves for nitrate and ammonium, as well as leachate nutrient concentration, were also measured in the sandy loam columns. All biochars significantly decreased the quantity of ammonium in the leachate, by 22 % to 78 %, and slowed its movement through the soil profile. Ammonium retention was linked to high cation exchange capacity and a high oxygen-to-carbon ratio, indicating that the primary control of ammonium retention in biochar-amended soils is the chemical affinity between biochar surfaces and ammonium. Biochars had little to no effect on the timing of nitrate release, and only SW500 decreased total quantity, by 27 % to 36 %. The ability of biochar to retain nitrate may be linked to high micropore specific surface area, suggesting a physical entrapment rather than a chemical binding. Together, this work sheds new light on the combined chemical and physical means by which biochar may alter soils to impact nutrient leaching and hydraulic conductivity for agricultural production.

## 1 Introduction

The ability of biochar to chemically and physically alter soil environments for specific agronomic benefits is the subject of increased investigation, as evidenced by the recent rise in published biochar studies (Web of Science, 2021) and United States trademark and patent applications listing the word “biochar” (US Patent and Trademark Office, 2021). Biochar, or the carbonaceous material created from the thermochemical conversion of biomass in an oxygen-limited environment (International Biochar Initiative, 2015), possesses unique chemical and physical properties, determined by variables such as its feedstock, production method, and production temperature. Biochar properties typically include a low bulk density, high porosity, high surface area, reactive surface functional groups, and recalcitrant carbon (Downie et al., 2009). These attributes make it a promising material for amendment to agricultural soils, as biochar may help improve soil water-holding capacity, hydraulic conductivity, and nutrient retention. Despite increased interest and investigation, there remains uncertainty regarding the ability of biochar to deliver these agronomic benefits. While many studies show promising results where nutrient retention and soil water dynamics are concerned (Blanco-Canqui, 2017; Glaser et al., 2002, 2015; Glaser and Lehr, 2019; Haider et al., 2020; Hestrin et al., 2019), others have demonstrated no or only minor effects (Griffin et al., 2017; Jones et al., 2012; Martos et al., 2020). Several authors have concluded that, due to differences in biochar production parameters and those of the soil environment, material- and site-specific investigation is required before conclusions can be drawn about the potential of biochar to provide agricultural benefits (Hassan et al., 2020; Jeffery et al., 2011; Zhang et al., 2016).

The ability of biochar to remove nitrate ( $\text{NO}_3^-$ ) and ammonium ( $\text{NH}_4^+$ ) from aqueous environments has been widely investigated, as it may indicate whether biochar can improve crop nutrient use efficiency and suppress fertilizer pollution through leaching and volatilization (Clough and Condon, 2010; Peiris et al., 2018). To this effect, batch sorption experiments are commonly carried out to determine the electrostatic affinity between biochars and  $\text{NO}_3^-$  and  $\text{NH}_4^+$ . The net charge of biochars varies based on their surface functional groups and the degree of protonation, as a function of soil pH and their point of zero charge (PZC). While biochar PZCs between 7 and 10 have been observed (Lu et al., 2013; Uchimiya et al., 2011), the high number of oxygen-containing functional groups (primarily carboxyl) typically led to PZCs of less than 5 (Peiris et al., 2019; Uchimiya et al., 2011; Wang et al., 2020). As such, the deprotonation of biochar surface functional groups occurs within most agronomic soils (pH  $\sim$  5–7.5), leading to a net negative charge. It is expected, then, that most biochars would not bind to  $\text{NO}_3^-$ , which exists in the anionic form in aqueous environments, while more readily binding to positively charged  $\text{NH}_4^+$  ions.

Electrostatic repulsion between  $\text{NO}_3^-$  and biochar has indeed been regularly cited as the reason behind little to no  $\text{NO}_3^-$  removal in batch sorption experiments. Zhou et al. (2019) tested biochars from four feedstocks, each produced at three temperatures, to find minimal  $\text{NO}_3^-$  sorption and even  $\text{NO}_3^-$  release. Similarly, Sanford et al. (2019) found that five biochars from diverse feedstocks and production temperatures had zero  $\text{NO}_3^-$  binding capacity. Little to no  $\text{NO}_3^-$  sorption capacity has been commonly observed for biochars produced from a broad range of feedstocks, production methods, and temperatures (Gai et al., 2014; Hale et al., 2013; Hollister et al., 2013; Li et al., 2018; Wang et al., 2017; Zeng et al., 2013). Though exceptions have been observed in which biochars exhibited high  $\text{NO}_3^-$  binding capacities (Ahmadvand et al., 2018; Chandra et al., 2020), a recent study determined the average published maximum adsorption capacity ( $Q_{\text{max}}$ ) of unmodified biochar for  $\text{NO}_3^-$ -N to be as low as  $1.95 \text{ mg g}^{-1}$  (Zhang et al., 2020).

This same study determined the average published  $Q_{\text{max}}$  of unmodified biochar for  $\text{NH}_4^+$ -N to be  $11.19 \text{ mg g}^{-1}$  (Zhang et al., 2020). Higher  $Q_{\text{max}}$  values for biochar and  $\text{NH}_4^+$  are to be expected, as  $\text{NH}_4^+$  exists in the cationic form in aqueous environments and would more readily adsorb to negatively charged biochar surfaces. While this theoretical electrostatic affinity is supported by higher  $Q_{\text{max}}$  values throughout published sorption experiments, inconsistencies can still be found.  $Q_{\text{max}}$  values lower than  $2 \text{ mg NH}_4^+ \text{ g}^{-1}$  are commonly observed, for biochars produced from a broad range of temperatures and feedstocks (Hale et al., 2013; Paramashivam et al., 2016; Song et al., 2019; Tian et al., 2016; Uttran et al., 2018; Wang et al., 2015a; Yin et al., 2019; Zhang et al., 2017). While most reported  $Q_{\text{max}}$  values are less than  $20 \text{ mg NH}_4^+ \text{ g}^{-1}$  (Zhang et al., 2020), higher values have been observed (Gao et al., 2015; Yin et al., 2018). Biochars exhibit a broad range of  $\text{NH}_4^+$  sorption capacities, and conflicting trends have emerged. Multiple authors have observed that sorption capacity decreases with increasing production temperature (Gai et al., 2014; Gao et al., 2015; Yin et al., 2018). Lower temperatures have been correlated with higher cation exchange capacity (CEC) (Gai et al., 2014), higher O/C ratios (Yang et al., 2017), and more abundant surface functional groups (Yin et al., 2018). These properties may contribute to biochars with enhanced ability to remove  $\text{NH}_4^+$  from solution, as they provide a greater number of exchange sites and oxygen-containing functional groups which can react with  $\text{NH}_4^+$  (Yang et al., 2017). The reverse trend has also been observed, however, with authors noting that an increase in production temperature resulted in higher  $\text{NH}_4^+$   $Q_{\text{max}}$  values (Chandra et al., 2020; Zeng et al., 2013; Zheng et al., 2013). Authors point towards the higher specific surface area (SSA) of biochar at higher production temperatures as a critical parameter to predicting  $\text{NH}_4^+$  adsorption.

Chemical bonding and electrostatic interactions may not be the only mechanism by which biochar retains  $\text{NO}_3^-$  and  $\text{NH}_4^+$  in soils. Despite the lack of chemical affinity between

$\text{NO}_3^-$  and biochar, studies frequently demonstrate the ability of biochar to inhibit  $\text{NO}_3^-$  leaching in soil column studies and pot trials (Haider et al., 2016; Kameyama et al., 2012; Pratiwi et al., 2016; Yao et al., 2012). While some authors hypothesize the mechanism to be microbial immobilization (Bu et al., 2017), others have found the addition of biochar to stimulate N mineralization (Teutscherova et al., 2018). In addition to chemical and microbial mechanisms, biochar may retain N through physical means (Clough and Condon, 2010). A literature review determined that biochar decreased soil bulk density by 3% to 31% and increased porosity by 14% to 64% (Blanco-Canqui, 2017). Biochar can also alter mean pore size and pore architecture, thereby influencing tortuosity and the residence time of water and nutrients within the soil profile (Lim et al., 2016; Quin et al., 2014). The impact of biochar on hydraulic conductivity appears dependent on soil texture, which highly influences pore structure. While exceptions have been observed, biochar has largely been shown to decrease the ability of a saturated soil to transmit water (saturated hydraulic conductivity ( $K_{\text{sat}}$ )) in coarse-textured soils and increase  $K_{\text{sat}}$  in finer soils (Blanco-Canqui, 2017). The impact of biochar on these soil physical properties may influence  $\text{NO}_3^-$  retention through a mechanism known as “nitrate capture”, in which  $\text{NO}_3^-$  molecules become physically entrapped within biochar pores (Haider et al., 2016), potentially leading to increased residence time in crop rooting zones and a greater opportunity for plant uptake (Haider et al., 2020; Kameyama et al., 2012, 2015).

In this project, biochar characterization, sorption, and soil column experiments were carried out using a robust matrix of commercially available biochars, produced from diverse feedstocks and at multiple temperatures. The suite of experiments was chosen in order to elucidate the degree to which these biochars (1) chemically bind  $\text{NO}_3^-$  and  $\text{NH}_4^+$ , (2) physically alter soil properties which influence saturated hydraulic conductivity, or (3) influence nutrient leaching, through either chemical or physical processes. This information was used to determine the biochar parameters that may optimize hydrologic and nutrient retention benefits in agricultural soils and to investigate the combination of chemical and physical mechanisms by which these benefits are delivered. Adding to the novelty of this project is that the same soils and biochars were used as those in ongoing 3-year field trials, so that mechanistic laboratory studies can be linked with effects observed in on-farm cropping systems. Results are intended to inform the production or modification of biochar for the delivery of agronomic benefits, as well as to improve predictions on the behavior of biochar in specific agricultural conditions.

## 2 Materials and methods

### 2.1 Biochar characterization

Seven biochars were obtained from the following feedstocks and produced at the following temperatures: almond shell at 500 °C (AS500, produced by Karr Group Co.), almond shell at 800 °C (AS800, Premier Mushroom and Community Power Co), coconut shell at 650 °C (CS650, Cool Planet), softwood at 500 °C (SW500, Karr Group Co.), softwood at 650 °C (SW650, Cool Planet), softwood at 800 °C (SW800, Pacific Biochar), and an additional softwood biochar produced at 500 °C and inoculated with a proprietary, yet commercially available, microbial formula (SW500-I, Karr Group Co.). Unless otherwise stated, biochars were sieved to 2 mm and characterized using procedures recommended by the International Biochar Initiative (2015): pH and electrical conductivity (EC) were measured at a 1 : 20 biochar to 18.2 M  $\Omega$  cm water (Barnstead Nanopore, Thermo Fisher) dilution ( $w : v$ ) after solutions were shaken for 90 min; total carbon, nitrogen, hydrogen, and oxygen were measured using a dry-combustion elemental analyzer (Costech ECS4010); and moisture, volatile, and ash content were measured as a percent of total dry weight through sequential shifts in furnace temperature (briefly, 2 h at 105 °C, 6 min at 950 °C, and 6 h at 750 °C, respectively) (ASTM D 1762-84, 2011). Particle size distribution was measured by laser diffraction (Coulter LS230). CEC was measured using a combination of the modified ammonium acetate compulsory displacement method (Gaskin et al., 2008) and the rapid saturation method (Mukome et al., 2013; Mulvaney et al., 2004): 0.25 g of biochar was leached with 18.2 M  $\Omega$  cm water ( $w : v$ ) under vacuum (−20 to −40 kPa). Leachate was stored and analyzed for dissolved organic carbon (DOC) through combustion (Shimadzu TOC-V). Biochar samples were then washed with 1 M sodium acetate (pH 8.2) until the EC of the elute was the same as the eluant. Samples were rinsed three times with 10 mL of 2-propanol then dried under vacuum for 10 min. To displace sodium ions, biochars were washed with 1 M ammonium acetate of the same volume as was required of sodium acetate. Leachate was collected and analyzed for sodium concentration through atomic absorption spectroscopy (Perkin Elmer AAnalyst 800). The micropore specific surface area ( $\text{SSA}_{\text{up}}$ ) was determined from  $\text{CO}_2$  adsorption isotherms at 273 K using nonlocal density functional theory (NLDFT) (Particle Testing Authority, Micromeritics TriStar II Plus 3.0, NLDFT model mod11.df2). Prior to analysis, samples were degassed with  $\text{N}_2$  at 393 K for 16 h.

Fourier transform infrared (FTIR) spectra of AS500, AS800, and SW500 biochars were collected using the diffuse reflectance infrared Fourier transform sampling mode (DRIFT; PIKE Technologies EasiDiff) with air-dried samples diluted to 3% with potassium bromide. All FTIR spectra were collected using a Thermo Nicolet 6700 FTIR spectrometer (Thermo Scientific) using 256 scans, 4  $\text{cm}^{-1}$  resolu-

tion, and a DTGS detector. FTIR bands were assigned as in Parikh et al. (2014). The PZC of AS500, AS800, and SW500 was estimated as the pH at which the zeta potential (ZP) was approximately zero, utilizing a ZetaPlus (Brookhaven Instruments Corp., Holtsville, NY) following the method established in Wang et al. (2016). Briefly, suspensions were prepared by adding 50 mL of 1 mM KCl to 0.1 g of biochar. Samples were sonicated for 1 h, and the pH was adjusted before ZP measurements by adding HCl or KOH dropwise. A total of 10 measurements were taken for each sample. Gross morphological differences among AS500, AS800, and SW500 were visualized by X-ray micro-computed tomography (X-ray microCT) at the Lawrence Berkeley National Laboratory Advance Light Source on beamline 8.3.2, using a beam energy of 21 KeV. Biochars were sieved to 2 mm and mounted in syringes of 8.3 mm diameter for imaging. A total of 1025 projections were acquired using continuous tomography mode with a 4× objective, for a final pixel size of 1.7 μm. Images were reconstructed using Gridrec methods via TomoPy and Xi-CAM (Gürsoy et al., 2014; Pandolfi et al., 2018). Image analysis was completed in Dragonfly, a 3D image analysis software free for noncommercial use (Object Research Systems, Canada).

## 2.2 Soil characterization

Hanford Sandy Loam (HSL) and Yolo Silt Loam (YSiL) soils were chosen for continuity between laboratory experiments and ongoing 3-year field trials utilizing the same biochars and soils. Collectively, these soils represent over 260 000 ha of arable land in California and offer textural distinctions within a range of soils commonly farmed in the Central Valley of California (Soil Survey Staff, 2014). Soils were located via Web Soil Survey (<http://websoilsurvey.sc.egov.usda.gov/>, last access: 1 May 2021) and collected from the top 30 cm in fallowed agricultural fields in Parlier, California (HSL), and Davis, California (YSiL). Soils were homogenized and sieved to 2 mm for characterization and column experiments. Colorimetric  $\text{NO}_3^-$  and  $\text{NH}_4^+$  measurements were made according to Doane and Horwath (2003) and Verdouw et al. (1978) (Shimadzu UV-1280). Extractable P was measured using the Olsen sodium bicarbonate extraction (Watanabe and Olsen, 1965). Concentrations of potassium, calcium, magnesium, and sodium were measured by extracting 4 g of soil with 40 mL of 1 M ammonium acetate on a shaker for 30 min. Nutrient concentrations of filtered extracts were determined through atomic absorption spectroscopy (Perkin Elmer AAnalyst 800). Total porosity was calculated from the pore volume divided by the total soil volume in representative cores. Pore volume was determined from the difference in weight between saturated and oven-dried (105 °C for 24 h) cores. The pH and EC of soils with and without biochar were measured via 1 : 2 soil to 18.2 M Ω cm water ( $w : v$ ) dilution, after 15 min on the shaker and 60 min at rest (Thomas, 1996). Soil texture analysis was performed by the Analytical Lab at

the University of California, Davis (Davis, CA, USA), using the hydrometer method (Sheldrick and Wang, 1993).

## 2.3 Sorption experiments

To investigate the ability of biochar to adsorb  $\text{NH}_4^+$  and  $\text{NO}_3^-$ , 0.1 g of biochar was added to 40 mL of solution containing either 0, 50, 100, 200, 400, or 600 mg L<sup>-1</sup> of  $\text{NO}_3^-$  (as  $\text{KNO}_3$ ) or  $\text{NH}_4^+$  (as  $\text{NH}_4\text{Cl}$ ), along with method blanks. All solutions were prepared in 0.1 mM NaCl and, as in Hale et al. (2013a), spiked at 1 % volume with a stock solution of 20 g L<sup>-1</sup> sodium azide to inhibit microbial growth. Monovalent NaCl was chosen to avoid cation bridging reactions during the experiment. All sorption experiments were performed in triplicate at 22 ± 1 °C. Tubes were placed on an end-over shaker at 8 rpm for 24 h. Supernatants were passed through a 0.45 μm filter and analyzed for colorimetric  $\text{NO}_3^-$  and  $\text{NH}_4^+$  (Shimadzu UV-1280) (Doane and Horwath, 2003; Verdouw et al., 1978). Single-point sorbed ion concentration was determined at initial concentrations of 100 mg  $\text{NO}_3^-$  or  $\text{NH}_4^+$  g<sup>-1</sup> biochar using Eq. (1).

$$q = \frac{C_0 V_0 - C_f V_f}{m}, \quad (1)$$

where  $q$  is the sorbed ion concentration (mg g<sup>-1</sup>),  $C_0$  and  $C_f$  are the initial and final sorbate concentrations, respectively (mg L<sup>-1</sup>),  $V_0$  and  $V_f$  are the initial and final solution volumes, respectively ( $L$ ), and  $m$  is the mass of biochar ( $g$ ). Langmuir, Freundlich, and Langmuir–Freundlich equations were tested to model the adsorption isotherms, with the Freundlich equation (Eq. 2) demonstrating the best fit based on  $r^2$  values.

$$q = K_f C_f^{\frac{1}{n}}, \quad (2)$$

where  $q$  and  $C_f$  are the same as in Eq. (1),  $K_f$  is the Freundlich constant (mg g<sup>-1</sup>), and  $\frac{1}{n}$  is the degree of nonlinearity of the isotherm. Excel was used to determine the parameters for the equations. Using batch sorption results, AS500, AS800, and SW500 were selected for further experimentation.

## 2.4 Column experiments

To investigate the influence of biochar on saturated hydraulic conductivity ( $K_{\text{sat}}$ ), constant head column experiments were performed in five replicates using the 5 station Chameleon Kit (Soilmoisture Equipment Corporation (SEC) 2816GX). SEC Tempe cells, each with a volume of 136.4 cm<sup>3</sup>, were packed with soils amended with 0 % and 2 % ( $w/w$ ) AS500, AS800, or SW500 biochars, to a bulk density of 1.34 ± 0.02 g cm<sup>-3</sup>. Soils and biochars were thoroughly and homogeneously mixed prior to being added to Tempe cells and packed using the dry method according to Gibert et al. (2014). An application rate of 2 % was chosen as the midrange of those represented in similar experiments (Blanco-Canqui, 2017) and is within recommended

ranges for field application (Guo, 2020; Jeffery et al., 2011). Columns were saturated for 24 h before the start of each experiment. Each column was gravity-fed a solution of 0.1 mM  $\text{CaCl}_2$  at a pressure head of 34 cm for 10 pore volumes. Divalent  $\text{CaCl}_2$  was chosen to avoid dispersion and the creation of preferential flow pathways.  $K_{\text{sat}}$  was calculated using data produced by SEC pressure transducers and PressureLogger software, which monitored pressure head and flow over time. Columns were also used to investigate nutrient retention and leaching in the HSL amended with 0 % and 2 % biochar.  $K_{\text{sat}}$  trials with the YSiL demonstrated that flow rates were very low ( $\sim 0.044 \text{ cm s}^{-1}$ ), creating logistical challenges for investigating nutrient retention and leaching in this soil. Additionally, the impact of  $\text{NO}_3^-$  leaching is more pronounced in coarsely textured soils. Thus, leaching experiments were conducted in HSL columns only. To remove existing nitrogen, columns were flushed for 10 pore volumes with 0.1 mM  $\text{CaCl}_2$ , after which  $50 \text{ mg L}^{-1}$  of both  $\text{NO}_3^-$  and  $\text{NH}_4^+$  (as  $\text{NH}_4\text{Cl}$  and  $\text{KNO}_3$ ) was gravity-fed through columns for 15 pore volumes. Leachate was collected every 0.5 pore volumes and analyzed for colorimetric  $\text{NO}_3^-$  and  $\text{NH}_4^+$  as in sorption experiments (Doane and Horwath, 2003; Verdouw et al., 1978).

## 2.5 Statistical analysis

All data were analyzed with linear models ( $\text{lm}(\text{response variable} \sim \text{biochar})$ ) and one-way analysis of variance (ANOVA) in the stats and Tidyverse packages in R (R Core Team, 2020; Wickham et al., 2019). When more than one soil type was tested (as in  $K_{\text{sat}}$  measurements), separate models were built for each soil type to determine the effect of biochar within soil types. For analysis of results, all effects with  $p$  values  $< 0.05$  were considered significant.  $P$  values were generated using the emmeans package in R (Lenth, 2019) and corrected for multiple comparisons using Tukey's honestly significant difference (HSD) method. Plots were generated in R using the ggplot2 package (Wickham, 2016) and visualized as the mean plus or minus the standard error (SE) of the means.

## 3 Results

### 3.1 Biochar characterization

Biochars exhibited a broad range of chemical and physical properties depending on their production temperature and feedstock (Tables 1 and 2). All biochars contained less than 1 % nitrogen, spanning from SW800 at 0.13 % to CS650 at 0.79 %. Almond shell biochars contained 4–6 times more nitrogen than softwood biochars produced at the same temperature. Softwood biochars produced at 500 and 800 °C had substantially higher  $\text{SSA}_{\text{up}}$  than almond shell biochars produced at the same temperatures. It should be noted, however, that  $\text{SSA}_{\text{up}}$  measured by  $\text{CO}_2$  adsorption frequently results in

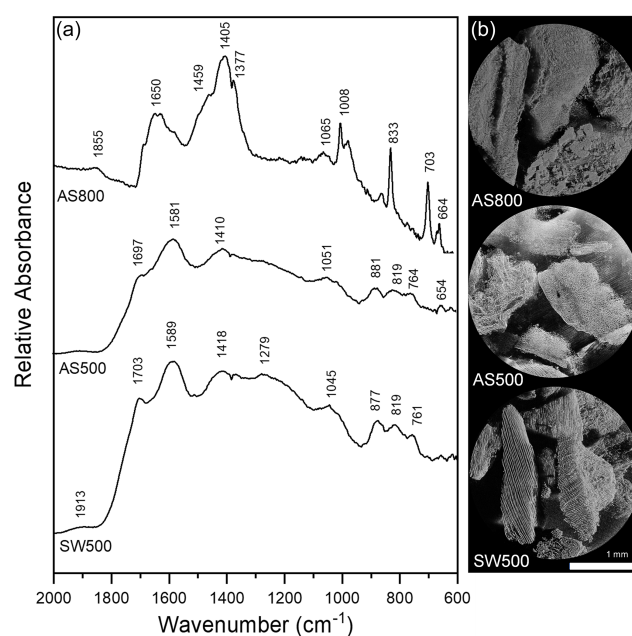


**Figure 1.** (a) DRIFT spectra of AS800, AS500, and SW500 biochars. Samples diluted with potassium bromide to 3 % sample and collected with  $256 \text{ cm}^{-1}$  scans with a  $4 \text{ cm}^{-1}$  resolution. (b) X-ray microCT images of AS800, AS500, and SW500 biochars.

higher values than surface area measured by  $\text{N}_2$ , as  $\text{CO}_2$  can access micropores unavailable to  $\text{N}_2$  (Maziarka et al., 2021; Zeng et al., 2013). While results from each method tend to be well correlated and are considered to provide complementary information (Sigmund et al., 2017), neither should be regarded as providing precise total surface area. Overall, AS800 possessed the most unique properties, with the lowest carbon content at 35.3 %, the highest ash content at 55.4 %, the highest EC at  $27.2 \text{ ms cm}^{-1}$ , a basic pH of 10.13, the highest O/C ratio at 0.56, and the second highest CEC at  $53.77 \text{ cmol}_c \text{ kg}^{-1}$ .

The IR spectra of AS500 and SW500 contained carboxyl and aromatic functional groups present at 1697 and  $1703 \text{ cm}^{-1}$  ( $\text{C}=\text{O}$ ) and 1410 and  $1418 \text{ cm}^{-1}$  ( $\text{COO}^-$ ), aromatic bands around  $1580 \text{ cm}^{-1}$   $\text{C}=\text{C}$  skeletal vibrations, out-of-plane  $\text{C}-\text{H}$  bending vibrations ( $700$  to  $900 \text{ cm}^{-1}$ ) associated with adjacent aromatic hydrogen bonds, and aromatic  $\text{C}=\text{C}$  and  $\text{C}=\text{O}$  stretching vibrations ( $1581$  and  $1589 \text{ cm}^{-1}$ ) (Fig. 1a, Table S1). AS800 spectra contained a strong band at  $1405 \text{ cm}^{-1}$ , representing substantial contributions of  $\text{COO}^-$ , and multiple sharp IR peaks from  $\sim 1000$  to  $700 \text{ cm}^{-1}$ , arising from metal oxide vibrations (Fig. 1a, Table S1). The high contribution of O-rich functional groups and metal oxide vibrations is consistent with the elemental analysis of AS800, which showed high oxygen and ash content (Table 1). The measured PZC for each of the three tested biochars is as follows: 3.2 for AS500, 6.8 for AS800, and 3.9 for SW500. The higher PZC of AS800 is consistent with the higher ash and

**Table 1.** Select chemical and physical biochar properties ( $n = 3$ )  $\pm$  SE of the means.

	AS500	AS800	CS650	SW500	SW500-I	SW650	SW800
Carbon (%)	65.8 $\pm$ 0.5	35.3 $\pm$ 0.3	71.2 $\pm$ 0.7	70.9 $\pm$ 0.3	63.5 $\pm$ 0.3	78.3 $\pm$ 0.4	41.8 $\pm$ 0.5
Nitrogen (%)	0.76 $\pm$ 0.01	0.55 $\pm$ 0.02	0.79 $\pm$ 0.04	0.13 $\pm$ 0.03	0.69 $\pm$ 0.01	0.29 $\pm$ 0.01	0.13 $\pm$ 0.03
Oxygen (%)	17.1 $\pm$ 0.8	26.4 $\pm$ 0.8	13.7 $\pm$ 0.6	17.1 $\pm$ 0.6	20.1 $\pm$ 0.2	10.2 $\pm$ 0.2	15.3 $\pm$ 0.9
Hydrogen (%)	3.1 $\pm$ 0.04	1.8 $\pm$ 0.02	3.2 $\pm$ 0.06	3.8 $\pm$ 0.01	3.8 $\pm$ 0.03	2.9 $\pm$ 0.07	1.5 $\pm$ 0.05
Molar O/C ratio	0.19 $\pm$ 0.01	0.56 $\pm$ 0.01	0.15 $\pm$ 0.01	0.18 $\pm$ 0.01	0.24 $\pm$ 0	0.1 $\pm$ 0	0.27 $\pm$ 0.01
Molar H/C ratio	0.55 $\pm$ 0.01	0.62 $\pm$ 0.01	0.54 $\pm$ 0.01	0.63 $\pm$ 0	0.71 $\pm$ 0.01	0.44 $\pm$ 0.01	0.42 $\pm$ 0.02
Volatile (%)	30.7 $\pm$ 2.7	28.2 $\pm$ 0.5	32.1 $\pm$ 0.4	38.0 $\pm$ 0.9	38.8 $\pm$ 1.2	26.9 $\pm$ 0.3	21.7 $\pm$ 0.2
Ash (%)	19.0 $\pm$ 1.0	5545 $\pm$ 0.8	5.3 $\pm$ 0.2	4.5 $\pm$ 0.1	9.2 $\pm$ 0.5	4.5 $\pm$ 0.3	31.5 $\pm$ 1.2
pH	9.3 $\pm$ 0.02	10.1 $\pm$ 0.01	7.8 $\pm$ 0.02	7.9 $\pm$ 0.02	10.4 $\pm$ 0.01	8.0 $\pm$ 0.03	10.3 $\pm$ 0.01
EC (ms cm <sup>-1</sup> )	3.2 $\pm$ 0.01	27.2 $\pm$ 0.1	0.3 $\pm$ 0	2.5 $\pm$ 0.02	2.1 $\pm$ 0.02	0.1 $\pm$ 0	2.1 $\pm$ 0.01
DOC (mg kg <sup>-1</sup> )	38 322.1 $\pm$ 1776.6	1055.9 $\pm$ 52.9	644.5 $\pm$ 77.1	43 776.2 $\pm$ 1103.8	32 171.2 $\pm$ 934.8	423.4 $\pm$ 50.6	475.2 $\pm$ 66.9
CEC (cmol <sub>c</sub> kg <sup>-1</sup> )	24.0 $\pm$ 0.6	52.7 $\pm$ 0.8	26.8 $\pm$ 1.1	16.5 $\pm$ 0.4	34.1 $\pm$ 0.2	21.7 $\pm$ 0.4	60.8 $\pm$ 0.8
Mean particle size ( $\mu$ m)	464.0	269.8	609.1	493.6	241.1	212.3	139.4
Median particle size ( $\mu$ m)	590.6	334.8	931.2	763.5	312.8	446.3	171.2
SSA <sub>up</sub> (m <sup>2</sup> g <sup>-1</sup> )	54.7	188.2	233.6	93.5	152.6	305.6	363.6

EC: electrical conductivity. DOC: dissolved organic carbon. CEC: cation exchange capacity. SSA<sub>up</sub>: micropore specific surface area.

metal-oxide content previously described. Each biochar was visually distinct at the macroscale (Fig. 1b). Animated reconstructions of biochar particles are provided in the Supplement (Fig. S1a–c). The macropores (> 50  $\mu$ m) of SW500 were more uniform in size compared to those of AS500 and AS800 (Figs. 1b, S1a–c). The softwood chips added to the AS500 feedstock matrix (at 25% *w/w* to assist with pyrolysis) are visible in the background and contrast sharply with the almond shells (Figs. 1b and S1a). The macropores of AS800 appeared to increase in size (most visible in the bottom right of AS800 Fig. 1a and in the animated reconstruction in Fig. S1b), due to the collapse of the lacy carbon pores that were visible in AS500 (Figs. 1b and S1a). The increase in production temperature resulted in more binomial pore size distribution in AS800, with larger macropores and an increased quantity of micropores, as observed by X-ray microCT and CO<sub>2</sub> SSA<sub>up</sub> measurements (Table 1, Figs. 1b, S1b), leading to an overall increase in total surface area.

### 3.2 Soil characterization

Table 2 contains select chemical and physical properties of soils used in this study. The finer textured YSiL had a porosity of 42.5%, a sand content of 24%, and a clay content of 33%, compared to the coarser HSL with a porosity of 29.9% and sand and clay contents of 59% and 12%, respectively. Both HSL and YSiL contained substantial levels of NO<sub>3</sub><sup>-</sup>, calcium, magnesium, and potassium and were slightly above neutral at a pH of 7.3.

All biochars exhibited the capacity to remove NH<sub>4</sub><sup>+</sup> from solution (Fig. 2), though  $K_f$  values were low (Table 3). Single-point concentration tests at a  $C_0$  of 100 mg L<sup>-1</sup> revealed the following hierarchy of sorption capacities, in order of lowest to highest: SW650 < SW500 < CS650 < SW500-I < AS500 < SW800 < AS800 (Table 3). These  $q$  values spanned 0.70 (SW650) to 7.15 (AS800) mg g<sup>-1</sup> or removal

**Table 2.** Select physical and chemical properties of Hanford Sandy Loam (HSL) and Yolo Silt Loam (YSiL) ( $n = 3$ )  $\pm$  SE of the means.

	HSL	YSiL
NH <sub>4</sub> <sup>+</sup> (mg kg <sup>-1</sup> )	0.74 $\pm$ 0.05	1.02 $\pm$ 0.14
NO <sub>3</sub> <sup>-</sup> (mg kg <sup>-1</sup> )	34.49 $\pm$ 0.50	40.40 $\pm$ 1.05
Ca (mg kg <sup>-1</sup> )	943.41 $\pm$ 11.56	2191.26 $\pm$ 7.19
Mg (mg kg <sup>-1</sup> )	58.05 $\pm$ 1.62	508.50 $\pm$ 11.60
K (mg kg <sup>-1</sup> )	55.91 $\pm$ 0.99	360.05 $\pm$ 0.70
Na (mg kg <sup>-1</sup> )	118.09 $\pm$ 2.27	146.56 $\pm$ 0.73
Olsen P (mg kg <sup>-1</sup> )	9.19 $\pm$ 0.12	9.83 $\pm$ 0.15
pH	7.3 $\pm$ 0.09	7.3 $\pm$ 0.05
EC ( $\mu$ s cm <sup>-1</sup> )	427.33 $\pm$ 2.84	269.25 $\pm$ 1.92
Porosity (%)	29.9 $\pm$ 0.35	42.5 $\pm$ 0.42
Sand (%)	59.0 $\pm$ 1.4	24.0 $\pm$ 0.9
Clay (%)	12.0 $\pm$ 0.9	33.0 $\pm$ 0.5

EC: electrical conductivity.

efficiencies of 0.70% and 7.15%. AS800 exhibited the greatest  $K_f$  value at 0.16 mg NH<sub>4</sub><sup>+</sup> g<sup>-1</sup>. Only AS500 exhibited the ability to remove NO<sub>3</sub><sup>-</sup> from solution. The other six biochars released, rather than removed, NO<sub>3</sub><sup>-</sup> (Fig. S1). For AS500, the single-point concentration test at a  $C_0$  of 100 mg L<sup>-1</sup> revealed a removal efficiency of 1.74% or a  $q$  of 1.74 mg g<sup>-1</sup> (Table 3). All tested models were poor fits for the AS500 and NO<sub>3</sub><sup>-</sup> isotherm, including the Freundlich equation with an  $r^2$  of 0.57. As such,  $K_f$  and  $\frac{1}{n}$  values provided in Table 3 should be regarded with caution.

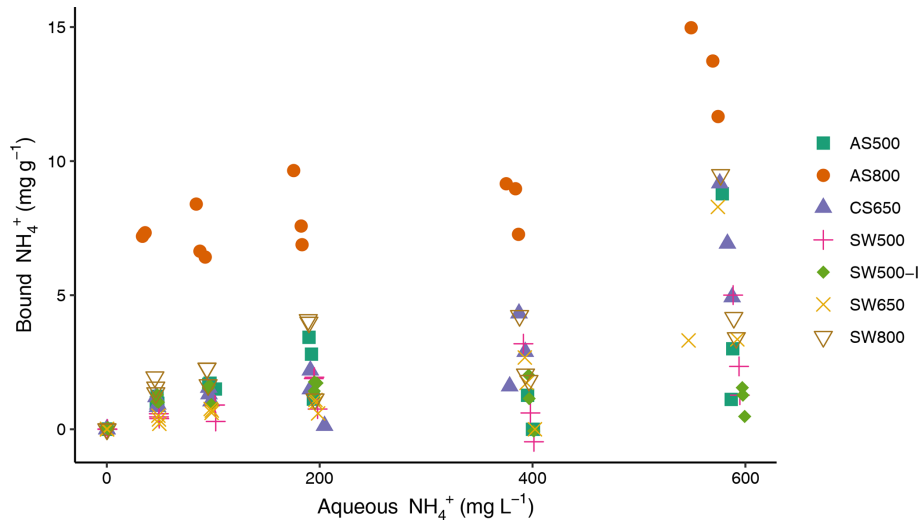


**Figure 2.** Sorption isotherms for ammonium and biochars, performed in triplicate at  $22 \pm 1$  °C. All solutions were prepared in 0.1 mM NaCl and spiked at 1 % volume with a stock solution of  $20 \text{ g L}^{-1}$  sodium azide to inhibit microbial growth.

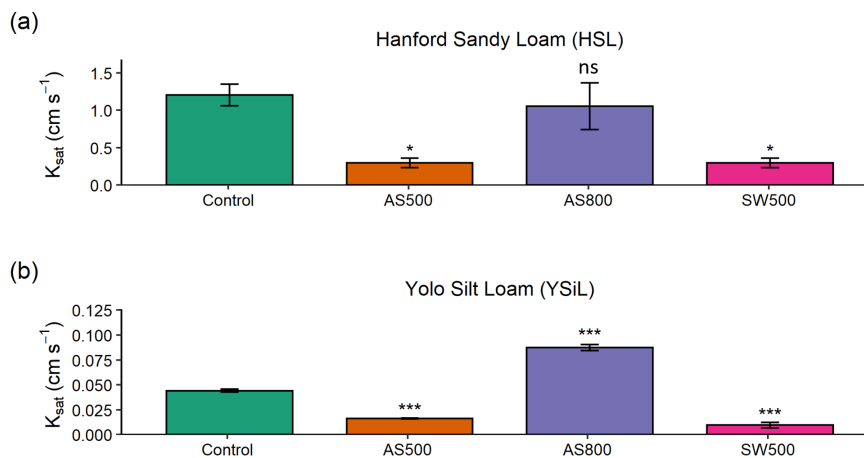


**Figure 3.** Impact of 0 % and 2 % addition of AS500, AS800, and SW500 biochars on saturated hydraulic conductivity ( $K_{\text{sat}}$ ) in (a) a Hanford Sandy Loam (HSL) soil and (b) a Yolo Silt Loam (YSiL) soil ( $n = 5$ ). Symbols denote significance levels as follows: n.s.: not significant, \*  $p < 0.05$ , \*\*  $p < 0.01$ , and \*\*\*  $p < 0.001$ .  $P$  values refer to comparisons between treatments and the control within each pore volume and were corrected for multiple comparisons using Tukey's HSD method.

### 3.3 Soil columns – hydraulic conductivity and breakthrough curves

There was a significant effect of biochar ( $p = 0.001$ ) on saturated hydraulic conductivity in both soils. In the HSL, AS500 and SW500 each decreased  $K_{\text{sat}}$  by 75 %, from the control at  $1.2$  to  $0.3 \text{ cm s}^{-1}$  ( $p = 0.023$ ) (Fig. 3). AS800 caused a 12.5 % decrease in  $K_{\text{sat}}$  to  $1.05 \text{ cm s}^{-1}$ , though the effect was not significant ( $p = 0.939$ ). In the YSiL, AS500 decreased  $K_{\text{sat}}$  by 63.6 %, from the control at  $0.044 \text{ cm s}^{-1}$  to  $0.016$  ( $p < 0.001$ ). SW500 caused a decrease of 79.5 % to  $0.009 \text{ cm s}^{-1}$  ( $p < 0.001$ ). In contrast to its effect on HSL,

AS800 increased  $K_{\text{sat}}$  in YSiL by 97.7 % to  $0.087 \text{ cm s}^{-1}$  ( $p < 0.001$ ).

Figure 4 illustrates the  $\text{NH}_4^+$  and  $\text{NO}_3^-$  breakthrough curves for HSL amended with 0 % and 2 % AS500, AS800, and SW500. Biochar affected the timing and quantity of  $\text{NH}_4^+$  (introduced in pore volumes 11–25 at  $50 \text{ mg L}^{-1}$ ) leached from the soil column (Fig. 4a). The estimated breakthrough point, or the pore volume at which the concentration of the leachate equals 0.5 times the concentration of the incoming solution ( $C/C_0 = 0.5$ ), was reached as follows, in order of fastest to slowest for  $\text{NH}_4^+$ : HSL (control) at pore volume 14.3, SW500 at 15.5, AS500 at

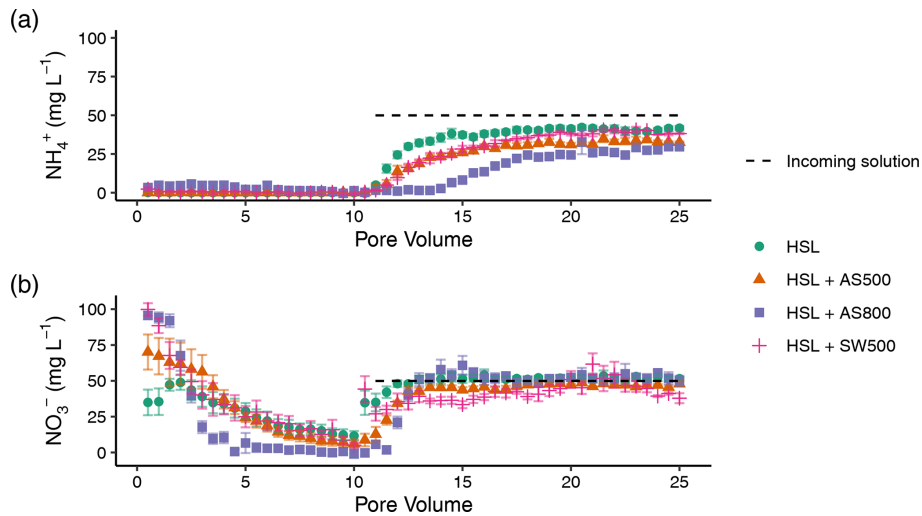


**Figure 4.** Breakthrough curves for (a) ammonium and (b) nitrate in a Hanford Sandy Loam (HSL) soil with 0 % and 2 % additions of AS500, AS800, and SW500 biochars. Native soil nitrogen was flushed in pore volumes 0–10 with a 0.1 mM CaCl<sub>2</sub> solution, after which 50 mg L<sup>-1</sup> solutions of NH<sub>4</sub><sup>+</sup> and NO<sub>3</sub><sup>-</sup> were gravity-fed through soil columns ( $n = 5$ ). Error bars represent standard error of the means.

**Table 3.** Concentration of ions bound to biochars (mg NH<sub>4</sub><sup>+</sup> or NO<sub>3</sub><sup>-</sup> g<sup>-1</sup>) at single-point concentration of 100 mg L<sup>-1</sup> and Freundlich model parameters ( $n = 3$ ). Nitrate parameters reported for only one biochar (AS500), as all other biochars released rather than removed NO<sub>3</sub><sup>-</sup>.

Biochar	Single-point concentration		Freundlich parameters		
	$q$ (mg NH <sub>4</sub> <sup>+</sup> g <sup>-1</sup> )	SE	$\frac{1}{n}$	$K_f$ (mg NH <sub>4</sub> <sup>+</sup> g <sup>-1</sup> )	$r^2$
AS500	1.63	0.05	0.71	0.05	0.90
AS800	7.15	0.51	0.77	0.16	0.84
CS650	1.30	0.12	0.65	0.06	0.75
SW500	0.70	0.17	0.83	0.01	0.91
SW500-I	1.37	0.18	0.52	0.08	0.73
SW650	0.69	0.03	0.68	0.03	0.89
SW800	2.06	0.17	0.77	0.04	0.90

Biochar	Single-point concentration		Freundlich parameters		
	$q$ (mg NO <sub>3</sub> <sup>-</sup> g <sup>-1</sup> )	SE	$\frac{1}{n}$	$K_f$ (mg NO <sub>3</sub> <sup>-</sup> g <sup>-1</sup> )	$r^2$
AS500	1.74	0.47	0.49	0.22	0.57

16.2, and AS800 at 18.1. Biochar also significantly decreased the total amount of NH<sub>4</sub><sup>+</sup> in the leachate at all pore volumes, as follows, in order of least to most retention: HSL < SW500 < AS500 < AS800 (Fig. 5a). At pore volume 15, AS500 decreased the NH<sub>4</sub><sup>+</sup> concentration of the leachate compared to the control (HSL = 37.33 mg L<sup>-1</sup>) by 30.5 % ( $p < 0.001$ ), AS800 by 78.1 % ( $p < 0.001$ ), and SW500 by 24.4 % ( $p = 0.002$ ). This effect was diminished by pore volume 25, where differences from the control (HSL = 41.69 mg L<sup>-1</sup>) were decreased to 21.8 % by AS500 ( $p < 0.001$ ), 28.9 % by AS800 ( $p < 0.001$ ), and 8.5 % by SW500 (not statistically significant at  $p = 0.463$ ).

Estimated NO<sub>3</sub><sup>-</sup> breakthrough points for biochar amended soils were each within 0.5 pore volumes of the control (pore

volume 11.4), indicating that biochar had little to no effect on the timing of NO<sub>3</sub><sup>-</sup> release from HSL. The effect of biochar on the total quantity of nitrate released was also less substantial than for NH<sub>4</sub><sup>+</sup> (Fig. 4b). Only SW500 significantly decreased the concentration of NO<sub>3</sub><sup>-</sup> in the leachate compared to the control. At pore volume 15, SW500 inhibited NO<sub>3</sub><sup>-</sup> transport by 35.01 % ( $p = 0.002$ ) (Fig. 5b). This effect was not present at pore volume 20 and was slightly lessened to 26.5 % by pore volume 25 (marginally significant at  $p = 0.098$ ).

Evaluation of data revealed no evidence of preferential flow in any replicate in any of the columns, which were carefully prepared according to the dry packing method in Gibert et al. (2014). This is demonstrated in the small error bars in figures of nutrient concentrations across pore volumes, as well as in hydraulic conductivity measurements taken by data loggers. To further monitor columns for preferential flow, the use of a conservative tracer could be considered in future experiments.

## 4 Discussion

### 4.1 Biochar properties and nutrient removal

An increase in biochar production temperature was generally associated with higher ash content, pH, EC, and surface area, as well as decreased carbon and hydrogen content and DOC. These trends are consistent with those of a recent meta-analysis of 533 published datasets (Hassan et al., 2020). Contrary to trends reported in the meta-analysis regarding high-temperature biochars, AS800 had a high O/C ratio and CEC (Hassan et al., 2020). The unusual O content of AS800 is attributed to the high ash content and is pos-

sibly due to oxidation through exposure to air immediately after gasification while still hot. As expected, the IR spectra of AS500 and SW500 were notably similar, having been produced at the same temperature by the same company via fractional hydrolysis. Additionally, the AS500 biochar included 25 % softwood chips to aid the pyrolysis process. By contrast, AS800 was produced via gasification and contained distinct peaks in the IR spectrum. This biochar also performed distinctly differently from other biochars in all experiments conducted.

The ability of all seven biochars to retain  $\text{NH}_4^+$  within the studied concentration ranges is consistent with a recent literature review of 77 studies (Zhang et al., 2020). AS800 exhibited substantially higher  $\text{NH}_4^+$  binding capacity than the other biochars tested. While it is typical for biochars produced at high temperatures to have low O/C ratios and low CEC (Hassan et al., 2020), AS800 had the largest O/C ratio at 0.56 (presumably due to the high ash content and possible post-pyrolysis oxidation) and the second highest CEC at  $52.75 \text{ cmol}_c \text{ kg}^{-1}$ . These properties, as well as the  $\nu_s$  ( $\text{COO}^-$ ) IR band at  $1405 \text{ cm}^{-1}$ , explain the high  $\text{NH}_4^+$  retention, as they indicate increased exchange sites and oxygen-containing functional groups which can react with  $\text{NH}_4^+$ . The relationship between these biochar properties and  $\text{NH}_4^+$  binding capacity was also demonstrated with SW800, which had the highest CEC at  $60.83 \text{ cmol}_c \text{ kg}^{-1}$ , the second highest O/C ratio at 0.27, and the second highest  $\text{NH}_4^+$  binding capacity. Consistent with prior biochar studies (Fidel et al., 2018; Georgiou et al., 2021; Hu et al., 2020; Jing et al., 2019), these data suggest that  $\text{NH}_4^+$  is bound to biochar through electrostatic interactions. The demonstrated relationship between  $\text{NH}_4^+$  sorption and large O/C ratios and CECs is also consistent with prior studies (Gai et al., 2014; Yang et al., 2017). By contrast, no clear trends between surface area (i.e.,  $\text{SSA}_{\text{up}}$ ) and  $\text{NH}_4^+$  retention emerged in this experiment, as observed in other studies (Chandra et al., 2020; Zeng et al., 2013; Zheng et al., 2013). However, Zeng et al. (2013) did observe that surface area and CEC were not consistently good predictors of  $\text{NH}_4^+$  and that other factors must be considered.

That six of the seven biochars did not retain  $\text{NO}_3^-$ , and in most cases released  $\text{NO}_3^-$ , is consistent with most published studies (Gai et al., 2014; Hale et al., 2013; Hollister et al., 2013; Li et al., 2018; Sanford et al., 2019; Wang et al., 2017; Zeng et al., 2013; Zhang et al., 2020; Zhou et al., 2019). Electrostatic repulsion is commonly cited as the mechanism, as most biochars contain carboxyl-rich surface functional groups and have PZCs below agronomic soil pH values (Peiris et al., 2019; Uchimiya et al., 2011; Wang et al., 2020). The PZC values obtained for AS500, AS800, and SW500 were indeed each lower than solution pH, indicating carboxyl functional groups were predominately deprotonated during sorption experiments. Despite a PZC of 3.2, AS500 exhibited minor affinity for  $\text{NO}_3^-$ . Though the data do not provide a clear mechanistic process, the relatively high

ash content and low CEC likely facilitated sorption via anionic binding, as positive charges from biochar ash could bind  $\text{NO}_3^-$ . This is consistent with data from prior studies (Wang et al., 2015b). While AS800 and SW800 had higher ash contents, they also had substantially greater CECs. Inhibited binding between the positively charged metals in the ash and the aqueous  $\text{NO}_3^-$  may be attributed to the electrostatic repulsion from deprotonated surface functional groups (Tan et al., 2020; Tong et al., 2019; Zhang et al., 2020).

#### 4.2 Column experiment – nutrient retention

As in sorption trials, AS800 retained the greatest quantity of  $\text{NH}_4^+$  in column studies, followed by AS500 and SW500. This suggests that the chemical affinity between biochar and  $\text{NH}_4^+$  is the controlling factor on the flow of  $\text{NH}_4^+$  through biochar-amended soils, as the order did not change between sorption and column experiments. By contrast, data indicate that the flow of  $\text{NO}_3^-$  may be dictated, though minor in effect, by physical means (Clough and Condron, 2010). This is consistent with a study which found no evidence of  $\text{NO}_3^-$  adsorption to corn stalk biochar surfaces but determined  $\text{NO}_3^-$  to be physically retained via diffusion into biochar or through interaction within biochar pores (Tong et al., 2019). Inconsistent with our results, however, the corn stalk biochar showed substantial retention of  $\text{NO}_3^-$ , though this study investigated pure biochar without soil, and a biochar produced from a different feedstock. Indeed, biochar feedstock has a profound impact on its porosity, with materials containing higher ash content typically leading to a lower total porosity biochar (Leng et al., 2021). Unlike in sorption trials, AS500 did not retain significant quantities of  $\text{NO}_3^-$ . This suggests a weak chemical affinity between AS500 and  $\text{NO}_3^-$ , in which  $\text{NO}_3^-$  was readily desorbed from AS500. Complete desorption between biochar and  $\text{NO}_3^-$  has been previously reported (Hale et al., 2013). SW500, however, significantly inhibited the flow of  $\text{NO}_3^-$ , despite not exhibiting chemical affinity in sorption trials. Wood biomass biochar produced at 400–700 °C has been noted as ideal for producing high-porosity biochars due to its low ash content, high lignin content, and preservation of its original pore structure (Leng et al., 2021). Thus, SW500 is predicted to have the highest total porosity of the three biochars used, partly due to macropore contributions as observed via X-ray microCT. This reinforces that nitrate capture likely occurred, in which nitrate retention is facilitated by increased surface area and porosity (Haider et al., 2016, 2020; Kameyama et al., 2012; Kammann et al., 2015).

Indeed, SW500 had a substantially larger  $\text{SSA}_{\text{up}}$  than AS500 ( $93.5$  compared to  $54.7 \text{ m}^2 \text{ g}^{-1}$ ). AS800, however, had an even greater  $\text{SSA}_{\text{up}}$  at  $188.2 \text{ m}^2 \text{ g}^{-1}$  but exhibited no capacity to retain  $\text{NO}_3^-$ , likely due to its high ash content and the formation of larger macropores pictured in X-ray microCT images (Fig. 1b), which are not probed via the  $\text{CO}_2$  surface area approach. Larger pores may have allowed water to move through the biochar more quickly and limited

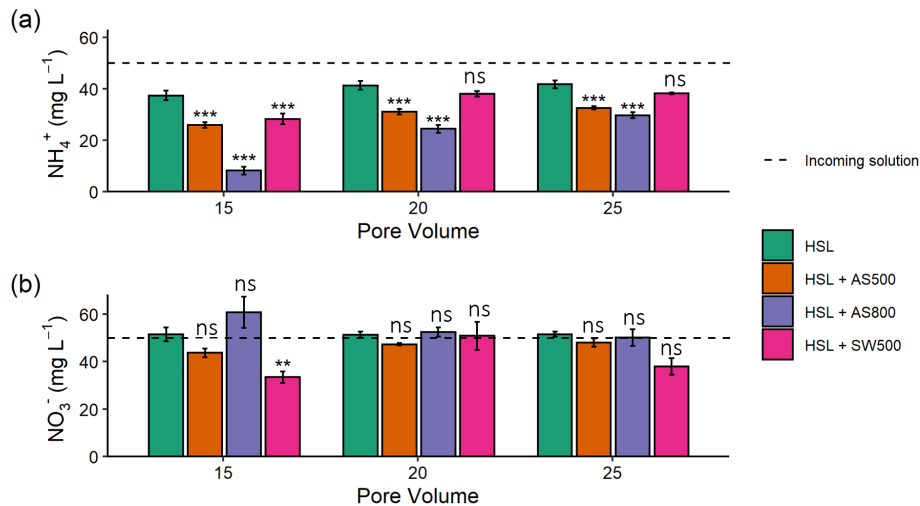


**Figure 5.** Quantity of (a) ammonium and (b) nitrate in Hanford Sandy Loam (HSL) soil columns with 0 % and 2 % additions of AS500, AS800, and SW500 biochars in pore volumes 15, 20, and 25 ( $n = 5$ ). Error bars represent standard error of the means. Symbols denote significance levels as follows: n.s.: not significant, \*  $p < 0.05$ , \*\*  $p < 0.01$ , and \*\*\*  $p < 0.001$ .  $P$  values refer to comparisons between treatments and the control within each pore volume and were corrected for multiple comparisons using Tukey's HSD method.

the flow of  $\text{NO}_3^-$  into micropores where it could be retained. This is consistent with the increase in soil  $K_{\text{sat}}$  after addition of AS800 in YSiL, and the smaller effect of AS800 in HSL compared to AS500 and SW500 (discussed in Sect. 4.3). Future investigation should include measurements of biochar surface area utilizing both  $\text{CO}_2$  and  $\text{N}_2$  adsorption. While  $\text{CO}_2$  is commonly used to probe micropores in carbon-based materials (Maziarka et al., 2021; Sigmund et al., 2017; Zhu et al., 2011), IBI criteria recommend the use of  $\text{N}_2$  for biochar analysis (International Biochar Initiative, 2015). Including  $\text{N}_2$  measurements would aid in standardization across studies. Furthermore, the differences in results from each method may be descriptive of the relative pore size distribution between each biochar in this study. Differences in pore size distributions, as observed by X-ray microCT, have been demonstrated to have a varying effect on water retention and conductivity in previous studies (Devereux et al., 2013; Quin et al., 2014). The strong  $\text{NH}_4^+$  binding capacity and high CEC of AS800 suggests a highly negatively charged surface. Electrostatic repulsion between AS800 and  $\text{NO}_3^-$ , therefore, may have also prevented nitrate capture. Together with sorption results, these breakthrough curves add to a growing body of literature which suggests that unmodified biochars may have a strong role in decreasing  $\text{NH}_4^+$  mobility in soils through chemical retention (Gai et al., 2014; Hale et al., 2013; Hollister et al., 2013; Li et al., 2018; Sanford et al., 2019; Wang et al., 2017; Zeng et al., 2013; Zhang et al., 2020; Zhou et al., 2019). Nitrate capture may have a role to play for reducing  $\text{NO}_3^-$  mobility but is unlikely to be a substantial force without chemical or physical modification of biochars. Modification of biochar has been shown to increase nutrient retention

(Zhang et al., 2020) and provides a promising opportunity to reduce  $\text{NO}_3^-$  leaching in agricultural soils.

#### 4.3 Column experiment – saturated hydraulic conductivity

AS500 and SW500 decreased  $K_{\text{sat}}$  by 75 % in HSL. AS800 also decreased  $K_{\text{sat}}$  in HSL, though to a lesser extent and without statistical significance. This effect is in agreement with a literature review of 26 similar studies, which consistently demonstrate decreased  $K_{\text{sat}}$  in coarse-textured soils after biochar amendment (Blanco-Canqui, 2017). This effect is hypothesized to be the result of increased surface area, microporosity, and tortuosity, which can slow the movement of water through soils. This decrease in  $K_{\text{sat}}$ , along with the prior discussion of SW500 porosity, further explains the retardation of  $\text{NO}_3^-$  transport in SW500 columns. By contrast, in fine-textured soils, biochar typically increases  $K_{\text{sat}}$  due to decreased bulk density and an increase in total porosity and mean pore size (Blanco-Canqui, 2017). This is consistent with the 98 % increase in  $K_{\text{sat}}$  in YSiL after amendment with AS800 but contrasts with the 64 % and 80 % reduction after the addition of AS500 and SW500, respectively. The microCT data show that AS800 has the most macropores which would permit greater water flow, whereas AS500 and SW500 have more micropores which can inhibit water flow due to matric forces greatly exceeding gravity forces. Though pore size was not quantitatively measured in this study, it is possible that the pores of AS500 and SW500 were small enough to decrease mean pore size in the coarse soil as in Devereux et al. (2013) but were not large or numerous enough to increase  $K_{\text{sat}}$  in a fine soil. By contrast, the collapse of the lacy carbon pores in the AS500 compared to AS800 led to

the formation of both additional small pores with greater surface area (confirmed by BET) and larger macropores (as visualized by X-ray microCT) in AS800. This may indicate an ability for AS800 to increase macroporosity, mean pore size, and pore connectivity in YSiL, as seen in other studies (Quin et al., 2014). Broadly, the ability of each biochar to substantially influence the movement of water through each soil underscores its effect on the physical composition of soils. This fact contributes to the hypothesis that  $\text{NO}_3^-$  capture may have occurred in the case of SW500.

#### 4.4 Implications for field conditions

Recent meta-analyses have concluded that biochar substantially increased soil water content at field capacity and permanent wilting point, in the field and lab, in coarse-textured soils only (Blanco-Canqui, 2017; Razzaghi et al., 2020). Despite these observed trends, benefits have been observed in fine-textured soils as well, including reduced crop water stress, increased yield (Kerré et al., 2017; Nawaz et al., 2019), and reduced crop loss during deficit irrigation (Madari et al., 2017). Other authors have reported little to no effect, or transient effects, of biochar on soil water dynamics in both fine- and coarse-textured soils (Jones et al., 2012; McDonald et al., 2019; Nelissen et al., 2015). The results of this study suggest these unmodified biochars may increase the residence time of water in sandy soils and increase drainage in fine-textured soils during irrigation or flooding events or when soils are otherwise saturated. Results also suggest biochar may increase the residence time of  $\text{NH}_4^+$  in neutral or basic soils. These effects may be particularly relevant for flooded agricultural systems such as rice, where  $\text{NH}_4^+$  is the primary source of N, and water retention is a key parameter for success (Minami, 1995). Indeed, 95 % of California rice production occurs in the Sacramento Valley, where both the YSiL and HSL soils are common ([http://rice.ucanr.edu/About\\_California\\_Rice/](http://rice.ucanr.edu/About_California_Rice/), last access: 1 June 2021). Data from these trials may help growers in regions with similar soil textures determine if biochar can increase water and nutrient retention in their systems. However, results cannot be extrapolated to dryland agriculture or in soils that experience wet–dry cycles, as unsaturated hydraulic conductivity was not measured. In order to determine how these biochars may behave in unsaturated conditions, 3-year processing tomato field trials are currently underway with the same biochars and soil textures. The intent is to observe the field-scale effects of these biochars on soil–water and nitrogen dynamics.

## 5 Conclusions

This study provides novel contributions to our understanding of biochar in soils by investigating the combination of chemical and physical mechanisms through which biochar influences nutrient retention and hydraulic conductivity and by in-

cluding a robust matrix of commercially available materials. Unmodified biochar was demonstrated to control the flow of  $\text{NH}_4^+$  primarily through chemical affinity. Ammonium retention was linked to biochar properties such as high CEC, O/C ratios, ash content, and the presence of oxygen-containing surface functional groups. Nitrate transport was shown to be influenced by physical rather than chemical means. This effect could perhaps be optimized by producing biochars, like SW500, which minimize CEC but maximize microporosity and surface area, to encourage the physical entrapment of  $\text{NO}_3^-$ . Biochar also had a large effect on saturated hydraulic conductivity, though this effect was not consistent across biochars and soils. Broadly, the results of this study suggest that biochar may increase the residence time of water in sandy soils and increase drainage in fine-textured soils, though soil- and biochar-specific investigation is required.

This study demonstrates that biochar can provide a suite of agronomic benefits, from nutrient retention to improvements in soil–water dynamics for crop production. Additional research and quantitative analysis at the micron and submicron scale is required to assess the influence of biochar on soil porosity and pore architecture. Field-scale investigation using these soils and biochars is also ongoing, in order to link the impact of biochar on hydraulic conductivity and nutrient leaching to its influence on crop yield and nutrient use efficiency. The findings from this study highlight the need to conduct similar laboratory and field experiments with tailored biochars for specific outcomes, such as for nutrient retention, where tailored biochars may have greater efficacy.

**Code and data availability.** All data that supported the results of this publication are publicly available under the Interdisciplinary Earth Data Alliance (IEDA) v1.0 (<https://doi.org/10.26022/IEDA/112008>, last access: 19 May 2021, Gelardi, 2021). Code is available from the corresponding author upon request.

**Supplement.** The supplement related to this article is available online at: <https://doi.org/10.5194/soil-7-811-2021-supplement>.

**Author contributions.** Funding acquisition was carried out by SJP. DLG, SJP, MAN, and DAR conceptualized and designed the experiments. SJP carried out FTIR analysis and data visualization. DAR captured and reconstructed microCT images. JEP conducted PZC analysis. All other experiments were carried out by DLG, under the supervision of SJP and MAN. DLG and IHA conducted formal analysis and data visualization. DLG prepared the manuscript, with equal contributions from all other co-authors.

**Competing interests.** The contact author has declared that neither they nor their co-authors have any competing interests.

**Disclaimer.** Publisher's note: Copernicus Publications remains neutral with regard to jurisdictional claims in published maps and institutional affiliations.

**Special issue statement.** This article is part of the special issue "Effects of wildfires and pyrogenic carbon on soil functioning and organic matter dynamics". It is not associated with a conference.

**Acknowledgements.** We are grateful to Cool Planet, Pacific Biochar, Karr Group Co., and Premier Mushroom for providing the biochars used in this study. We would like to thank Dula Parkinson and Andrew McElrone for their assistance at the Lawrence Berkeley National Laboratory Advanced Light Source (ALS) Beamline 8.3.2 microtomography facility. We are grateful to Mike Marsh and the staff at Object Research Systems for providing a license for Dragonfly software and for the technical support in reconstructing and interpreting microCT images. Thanks are also given to the Davis R Users group for statistical and coding consultation and to Tad Doane and Alex Barbour for laboratory support.

**Financial support.** This publication was made possible by funding from the California Department of Food and Agriculture Fertilizer Research and Education Program (16-0662-SA-0), the Almond Board of California (17-ParikhS-COC-01), and the United States Department of Agriculture (USDA), National Institute of Food and Agriculture (NIFA) through Hatch Formula Funding (CA 2076-H) and a multistate regional project (W-3045). ALS is supported by the Director, Office of Science, Office of Basic Energy Science, of the US Department of Energy, under contract no. DE-AC02-05CH11231. Additionally, this research was supported by the UC Davis Dissertation Year Fellowship, a Henry A. Jastro Graduate Research Award, the Beatrice Oberly and S. Atwood McKeehan Fellowship, and the Foundation for Food and Agriculture Research Fellowship.

**Review statement.** This paper was edited by Gabriel Sigmund and reviewed by two anonymous referees.

## References

- Ahmadvand, M., Soltani, J., Ebrahim, S., Garmdareh, H., and Varavipour, M.: The relationship between the characteristics of Biochar produced at different temperatures and its impact on the uptake of NO<sub>3</sub>-N, *Environ. Heal. Eng. Manag. J.*, 5, 67–75, <https://doi.org/10.15171/EHEM.2018.10.2018>.
- ASTM D 1762-84: Standard Test Method for Chemical Analysis of Wood Charcoal., ASTM Int., 84(Reapproved 2007), 1–2, <https://doi.org/10.1520/D1762-84R07.2>, 2011.
- Blanco-Canqui, H.: Biochar and Soil Physical Properties, *Soil Sci. Soc. Am. J.*, 81, 687–711, <https://doi.org/10.2136/sssaj2017.01.0017>, 2017.
- Bu, X., Xue, J., Zhao, C., Wu, Y., and Han, F.: Nutrient Leaching and Retention in Riparian Soils as Influ-

- enced by Rice Husk Biochar Addition, *Soil Sci.*, 182, 1, <https://doi.org/10.1097/ss.0000000000000217>, 2017.
- Chandra, S., Medha, I., and Bhattacharya, J.: Potassium-iron rice straw biochar composite for sorption of nitrate, phosphate, and ammonium ions in soil for timely and controlled release, *Sci. Total Environ.*, 712, 136337, <https://doi.org/10.1016/j.scitotenv.2019.136337>, 2020.
- Clough, T. J. and Condon, L. M.: Biochar and the Nitrogen Cycle: Introduction, *J. Environ. Qual.*, 39, 1218, <https://doi.org/10.2134/jeq2010.0204>, 2010.
- Devereux, R. C., Sturrock, C. J., and Mooney, S. J.: The effects of biochar on soil physical properties and winter wheat growth, *Earth Env. Sci. T. R. So.*, 103, 13–18, <https://doi.org/10.1017/S1755691012000011>, 2013.
- Doane, T. A. and Horwath, W. R.: Spectrophotometric determination of nitrate with a single reagent, *Anal. Lett.*, <https://doi.org/10.1081/AL-120024647>, 2003.
- Downie, A., Crosky, A., and Munroe, P.: Characteristics of biochar – physical and structural properties, *Biochar Environ. Manag. Sci. Technol.*, 1, 89–108, <https://doi.org/10.4324/9780203762264>, 2009.
- Fidel, R. B., Laird, D. A., and Spokas, K. A.: Sorption of ammonium and nitrate to biochars is electrostatic and pH-dependent, *Sci. Rep.*, 8, 17627, <https://doi.org/10.1038/s41598-018-35534-w>, 2018.
- Gai, X., Wang, H., Liu, J., Zhai, L., Liu, S., Ren, T., and Liu, H.: Effects of feedstock and pyrolysis temperature on biochar adsorption of ammonium and nitrate, *PLoS One*, 9, 1–19, <https://doi.org/10.1371/journal.pone.0113888>, 2014.
- Gao, F., Xue, Y., Deng, P., Cheng, X., and Yang, K.: Removal of aqueous ammonium by biochars derived from agricultural residuals at different pyrolysis temperatures, *Chem. Speciat. Bioavailab.*, 27, 92–97, <https://doi.org/10.1080/09542299.2015.1087162>, 2015.
- Gaskin, J. W., Steiner, C., Harris, K., Das, K. C., and Bibens, B.: Effect of Low-Temperature Pyrolysis Conditions on Biochar for Agricultural Use, *Trans. ASABE*, 51, 2061–2069, <https://doi.org/10.13031/2013.25409>, 2008.
- Gelardi, D. L.: Biochar alters hydraulic conductivity and inhibits nutrient leaching in two agricultural soils, Version 1.0, Interdisciplinary Earth Data Alliance (IEDA) [data set], <https://doi.org/10.26022/IEDA/112008>, last access: 19 May 2021.
- Georgiou, E., Mihajlović, M., Petrović, J., Anastopoulos, I., Dosche, C., Pashalidis, I., and Kalderis, D.: Single-stage production of miscanthus hydrochar at low severity conditions and application as adsorbent of copper and ammonium ions, *Bioresour. Technol.*, 337, 125458, <https://doi.org/10.1016/j.biortech.2021.125458>, 2021.
- Gibert, O., Hernández, M., Vilanova, E., and Cornellà, O.: Guideline protocol for soil-column experiments assessing fate and transport of trace organics, *Demeau, Brussels, Belgium*, 3, 54 pp., 2014.
- Glaser, B. and Lehr, V. I.: Biochar effects on phosphorus availability in agricultural soils: A meta-analysis, *Sci. Rep.*, 9, 1–9, <https://doi.org/10.1038/s41598-019-45693-z>, 2019.
- Glaser, B., Lehmann, J., and Zech, W.: Ameliorating physical and chemical properties of highly weathered soils in the trop-

- ics with charcoal – A review, *Biol. Fertil. Soils*, 35, 219–230, <https://doi.org/10.1007/s00374-002-0466-4>, 2002.
- Glaser, B., Wiedner, K., Seelig, S., Schmidt, H. P., and Gerber, H.: Biochar organic fertilizers from natural resources as substitute for mineral fertilizers, *Agr. Sustain. Dev.*, 35, 667–678, <https://doi.org/10.1007/s13593-014-0251-4>, 2015.
- Griffin, D. E., Wang, D., Parikh, S. J., and Scow, K. M.: Short-lived effects of walnut shell biochar on soils and crop yields in a long-term field experiment, *Agr. Ecosyst. Environ.*, 236, 21–29, <https://doi.org/10.1016/j.agee.2016.11.002>, 2017.
- Guo, M.: The 3r principles for applying biochar to improve soil health, *Soil Syst.*, 4, 1–16, <https://doi.org/10.3390/soilsystems4010009>, 2020.
- Gürsoy, D., De Carlo, F., Xiao, X., and Jacobsen, C.: TomoPy: A framework for the analysis of synchrotron tomographic data, *J. Synchrotron Radiat.*, 21, 1188–1193, <https://doi.org/10.1107/S1600577514013939>, 2014.
- Haider, G., Steffens, D., Müller, C., and Kammann, C. I.: Standard Extraction Methods May Underestimate Nitrate Stocks Captured by Field-Aged Biochar, *J. Environ. Qual.*, 45, 1196–1204, <https://doi.org/10.2134/jeq2015.10.0529>, 2016.
- Haider, G., Joseph, S., Steffens, D., Müller, C., Taherymoosavi, S., Mitchell, D., and Kammann, C. I.: Mineral nitrogen captured in field-aged biochar is plant-available, *Sci. Rep.*, 10, 1–12, <https://doi.org/10.1038/s41598-020-70586-x>, 2020.
- Hale, S. E., Alling, V., Martinsen, V., Mulder, J., Breedveld, G. D., and Cornelissen, G.: The sorption and desorption of phosphate-P, ammonium-N and nitrate-N in cacao shell and corn cob biochars, *Chemosphere*, 91, 1612–1619, <https://doi.org/10.1016/j.chemosphere.2012.12.057>, 2013.
- Hassan, M., Liu, Y., Naidu, R., Parikh, S. J., Du, J., Qi, F., and Willett, I. R.: Influences of feedstock sources and pyrolysis temperature on the properties of biochar and functionality as adsorbents: A meta-analysis, *Sci. Total Environ.*, 744, 140714, <https://doi.org/10.1016/j.scitotenv.2020.140714>, 2020.
- Hestrin, R., Torres-Rojas, D., Dynes, J. J., Hook, J. M., Regier, T. Z., Gillespie, A. W., Smernik, R. J., and Lehmann, J.: Fire-derived organic matter retains ammonia through covalent bond formation, *Nat. Commun.*, 10, 1–8, <https://doi.org/10.1038/s41467-019-08401-z>, 2019.
- Hollister, C. C., Bisogni, J. J., and Lehmann, J.: Ammonium, Nitrate, and Phosphate Sorption to and Solute Leaching from Biochars Prepared from Corn Stover (*Zea mays* L.) and Oak Wood (*Quercus* spp.), *J. Environ. Qual.*, 42, 137–144, <https://doi.org/10.2134/jeq2012.0033>, 2013.
- Hu, X., Zhang, X., Ngo, H. H., Guo, W., Wen, H., Li, C., Zhang, Y., and Ma, C.: Comparison study on the ammonium adsorption of the biochars derived from different kinds of fruit peel, *Sci. Total Environ.*, 707, 135544, <https://doi.org/10.1016/j.scitotenv.2019.135544>, 2020.
- International Biochar Initiative: Standardized Product Definition and Product Testing Guidelines for Biochar That Is Used in Soil, *Int. Biochar Initiat.* (November), available at: <http://www.biochar-international.org/characterizationstandard> (last access: 20 April 2020), 2015.
- Jeffery, S., Verheijen, F. G. A., van der Velde, M., and Bastos, A. C.: A quantitative review of the effects of biochar application to soils on crop productivity using meta-analysis, *Agr. Ecosyst. Environ.*, 144, 175–187, <https://doi.org/10.1016/j.agee.2011.08.015>, 2011.
- Jing, H. P., Li, Y., Wang, X., Zhao, J., and Xia, S.: Simultaneous recovery of phosphate, ammonium and humic acid from wastewater using a biochar supported Mg(OH)<sub>2</sub>/bentonite composite, *Environ. Sci. Water Res. Technol.*, 5, 931–943, <https://doi.org/10.1039/c8ew00952j>, 2019.
- Jones, D. L., Rousk, J., Edwards-Jones, G., DeLuca, T. H., and Murphy, D. V.: Biochar-mediated changes in soil quality and plant growth in a three year field trial, *Soil Biol. Biochem.*, 45, 113–124, <https://doi.org/10.1016/j.soilbio.2011.10.012>, 2012.
- Kameyama, K., Miyamoto, T., Shiono, T., and Shinogi, Y.: Influence of Sugarcane Bagasse-derived Biochar Application on Nitrate Leaching in Calcaric Dark Red Soil, *J. Environ. Qual.*, 41, 1131–1137, <https://doi.org/10.2134/jeq2010.0453>, 2012.
- Kammann, C. I., Schmidt, H. P., Messerschmidt, N., Linsel, S., Steffens, D., Müller, C., Koyro, H. W., Conte, P., and Stephen, J.: Plant growth improvement mediated by nitrate capture in co-composted biochar, *Sci. Rep.*, 5, 1–13, <https://doi.org/10.1038/srep11080>, 2015.
- Kerré, B., Willaert, B., Cornelis, Y., and Smolders, E.: Long-term presence of charcoal increases maize yield in Belgium due to increased soil water availability, *Eur. J. Agron.*, 91, 10–15, <https://doi.org/10.1016/j.eja.2017.09.003>, 2017.
- Leng, L., Xiong, Q., Yang, L., Li, H., Zhou, Y., Zhang, W., Jiang, S., Li, H., and Huang, H.: An overview on engineering the surface area and porosity of biochar, *Sci. Total Environ.*, 763, 144204, <https://doi.org/10.1016/j.scitotenv.2020.144204>, 2021.
- Lenth, R.: Emmeans: estimated marginal means, Aka Least-Squares Means., available at: <https://cran.r-project.org/package=emmeans> (last access: 1 April 2020), 2019.
- Li, S., Barreto, V., Li, R., Chen, G., and Hsieh, Y. P.: Nitrogen retention of biochar derived from different feedstocks at variable pyrolysis temperatures, *J. Anal. Appl. Pyrolysis*, 133, 136–146, <https://doi.org/10.1016/j.jaap.2018.04.010>, 2018.
- Lim, T. J., Spokas, K. A., Feyereisen, G., and Novak, J. M.: Predicting the impact of biochar additions on soil hydraulic properties, *Chemosphere*, 142, 136–144, <https://doi.org/10.1016/j.chemosphere.2015.06.069>, 2016.
- Lu, H., Zhang, W., Wang, S., Zhuang, L., Yang, Y., and Qiu, R.: Characterization of sewage sludge-derived biochars from different feedstocks and pyrolysis temperatures, *J. Anal. Appl. Pyrolysis*, 102, 137–143, <https://doi.org/10.1016/j.jaap.2013.03.004>, 2013.
- Madari, B. E., Silva, M. A. S., Carvalho, M. T. M., Maia, A. H. N., Petter, F. A., Santos, J. L. S., Tsai, S. M., Leal, W. G. O., and Zeviani, W. M.: Properties of a sandy clay loam Haplic Ferralsol and soybean grain yield in a five-year field trial as affected by biochar amendment, *Geoderma*, 305, 100–112, <https://doi.org/10.1016/j.geoderma.2017.05.029>, 2017.
- Martos, S., Mattana, S., Ribas, A., Albanell, E., and Domene, X.: Biochar application as a win-win strategy to mitigate soil nitrate pollution without compromising crop yields: a case study in a Mediterranean calcareous soil, *J. Soils Sediments*, 20, 220–233, <https://doi.org/10.1007/s11368-019-02400-9>, 2020.
- Maziarka, P., Wurzer, C., Arauzo, P. J., Dieguez-Alonso, A., Mašek, O., and Ronsse, F.: Do you BET on routine?, The reliability of N<sub>2</sub> physisorption for the quantitative assessment of biochar's surface area, *Chem. Eng. J.*, 418, 129234, <https://doi.org/10.1016/j.cej.2021.129234>, 2021.

- McDonald, M. R., Bakker, C., and Motior, M. R.: Evaluation of wood biochar and compost soil amendment on cabbage yield and quality, *Can. J. Plant Sci.*, 99, 624–638, <https://doi.org/10.1139/cjps-2018-0122>, 2019.
- Minami, K.: The effect of nitrogen fertilizer use and other practices on methane emission from flooded rice, *Fertil. Res.*, 40, 71–84, <https://doi.org/10.1007/BF00749864>, 1995.
- Mukome, F. N. D., Zhang, X., Silva, L. C. R., Six, J., and Parikh, S. J.: Use of chemical and physical characteristics to investigate trends in biochar feedstocks, *J. Agric. Food Chem.*, 61, 2196–2204, <https://doi.org/10.1021/jf3049142>, 2013.
- Mulvaney, R. L., Yaremych, S. A., Khan, S. A., Swiader, J. M., and Horgan, B. P.: Use of Diffusion to Determine Soil Cation-Exchange Capacity by Ammonium Saturation, *Commun. Soil Sci. Plant Anal.*, 35, 51–67, <https://doi.org/10.1081/CSS-120027634>, 2004.
- Nawaz, H., Hussain, N., Akbar Anjum, M., Rehman, H., Jamil, M., Aown Sammar Raza, M., and Farooq, O.: Biochar Application Improves the Wheat Productivity under Different Irrigation Water-Regimes, *Intl. J. Agric. Biol.*, 21, 936–942, <https://doi.org/10.17957/IJAB/15.0978>, 2019.
- Nelissen, V., Ruyschaert, G., Manka'Abusi, D., D'Hose, T., De Beuf, K., Al-Barri, B., Cornelis, W., and Boeckx, P.: Impact of a woody biochar on properties of a sandy loam soil and spring barley during a two-year field experiment, *Eur. J. Agron.*, 62, 65–78, <https://doi.org/10.1016/j.eja.2014.09.006>, 2015.
- Pandolfi, R. J., Allan, D. B., Arenholz, E., Barroso-Luque, L., Campbell, S. I., Caswell, T. A., Blair, A., De Carlo, F., Fackler, S., Fournier, A. P., Freychet, G., Fukuto, M., Gürsoy, D., Jiang, Z., Krishnan, H., Kumar, D., Kline, R. J., Li, R., Liman, C., Marchesini, S., Mehta, A., N'Diaye, A. T., Parkinson, D. Y., Parks, H., Pellouchoud, L. A., Perciano, T., Ren, F., Sahoo, S., Strzalka, J., Sunday, D., Tassone, C. J., Ushizima, D., Venkatakishnan, S., Yager, K. G., Zwart, P., Sethian, J. A., and Hexemer, A.: Xi-cam: a versatile interface for data visualization and analysis, *J. Synchrotron Radiat.*, 25, 1261–1270, <https://doi.org/10.1107/S1600577518005787>, 2018.
- Paramashivam, D., Clough, T. J., Dickinson, N. M., Horswell, J., Lense, O., Clucas, L., and Robinson, B. H.: Effect of Pine Waste and Pine Biochar on Nitrogen Mobility in Biosolids, *J. Environ. Qual.*, 45, 360–367, <https://doi.org/10.2134/jeq2015.06.0298>, 2016.
- Parikh, S. J., Goyne, K. W., Margenot, A. J., Mukome, F. N. D., and Calderón, F. J.: Soil Chemical Insights Provided through Vibrational Spectroscopy Publications from USDA-ARS/UNL Faculty. Paper 1471, available at: <http://digitalcommons.unl.edu/usdaarsfacpub/1471> (last access: 1 April 2021), 2014.
- Peiris, C., Gunatilake, S. R., Wewalwela, J. J., and Vithanage, M.: Biochar for sustainable agriculture: Nutrient dynamics, soil enzymes, and crop growth, Elsevier Inc., 211–224, 2018.
- Peiris, C., Nayanathara, O., Navarathna, C. M., Jayawardhana, Y., Nawalage, S., Burk, G., Karunanayake, A. G., Madduri, S. B., Vithanage, M., Kaumal, M. N., Mlsna, T. E., Hassan, E. B., Abeyundara, S., Ferez, F., and Gunatilake, S. R.: The influence of three acid modifications on the physicochemical characteristics of tea-waste biochar pyrolyzed at different temperatures: A comparative study, *RSC Adv.*, 9, 17612–17622, <https://doi.org/10.1039/c9ra02729g>, 2019.
- Pratiwi, E. P. A., Hillary, A. K., Fukuda, T., and Shinogi, Y.: The effects of rice husk char on ammonium, nitrate and phosphate retention and leaching in loamy soil, *Geoderma*, 277, 61–68, <https://doi.org/10.1016/j.geoderma.2016.05.006>, 2016.
- Quin, P. R., Cowie, A. L., Flavel, R. J., Keen, B. P., Macdonald, L. M., Morris, S. G., Singh, B. P., Young, I. M., and Van Zwiiten, L.: Oil mallee biochar improves soil structural properties-A study with x-ray micro-CT, *Agr. Ecosyst. Environ.*, 191, 142–149, <https://doi.org/10.1016/j.agee.2014.03.022>, 2014.
- R Core Team: R: A language and environment for statistical computing, available at: <https://www.r-project.org/>, last access: 15 April 2020.
- Razzaghi, F., Obour, P. B., and Arthur, E.: Does biochar improve soil water retention?, A systematic review and meta-analysis, *Geoderma*, 361, 114055, <https://doi.org/10.1016/j.geoderma.2019.114055>, 2020.
- Sanford, J. R., Larson, R. A., and Runge, T.: Nitrate sorption to biochar following chemical oxidation, *Sci. Total Environ.*, 669, 938–947, <https://doi.org/10.1016/j.scitotenv.2019.03.061>, 2019.
- Sheldrick, B. H. and Wang, C.: Particle Size Distribution, Lewis Publications/CRC Press, Boca Raton, FL, 499–511, 1993.
- Sigmund, G., Hüffer, T., Hofmann, T., and Kah, M.: Biochar total surface area and total pore volume determined by N<sub>2</sub> and CO<sub>2</sub> physisorption are strongly influenced by degassing temperature, *Sci. Total Environ.*, 580, 770–775, <https://doi.org/10.1016/j.scitotenv.2016.12.023>, 2017.
- Soil Survey Staff: Web Soil Survey, Natural Resources Conservation Service, United States Department of Agriculture, Nat. Resour. Conserv. Serv. United States Dep. Agric., 1–2, available at: <http://websoilsurvey.nrcs.usda.gov/> (last access: 1 January 2021), 2014.
- Song, H., Wang, J., Garg, A., Lin, X., Zheng, Q., and Sharma, S.: Potential of novel biochars produced from invasive aquatic species outside food chain in removing ammonium nitrogen: Comparison with conventional biochars and clinoptilolite, *Sustain.*, 11, 1–18, <https://doi.org/10.3390/su11247136>, 2019.
- Tan, G., Mao, Y., Wang, H., and Xu, N.: A comparative study of arsenic(V), tetracycline and nitrate ions adsorption onto magnetic biochars and activated carbon, *Chem. Eng. Res. Des.*, 159, 582–591, <https://doi.org/10.1016/j.cherd.2020.05.011>, 2020.
- Teutscherova, N., Houska, J., Navas, M., Masaguer, A., Benito, M., and Vazquez, E.: Leaching of ammonium and nitrate from Acrisol and Calcisol amended with holm oak biochar: A column study, *Geoderma*, 323, 136–145, <https://doi.org/10.1016/j.geoderma.2018.03.004>, 2018.
- Thomas, G. W.: Soil pH and soil acidity in: *Methods of Soil Analysis: Part 3 Chemical Methods*, edited by: Sparks, D. L., Page, A. L., Helmke, P. A., Loeppert, R. H., Soltanpour, P. N., Tabatabai, M. A., Johnston, C. T., and Summer, M. E., American Society of Agronomy Inc., Soil Science Society of America, Madison, WI., 475–490, 1996.
- Tian, J., Miller, V., Chiu, P. C., Maresca, J. A., Guo, M., and Imhoff, P. T.: Nutrient release and ammonium sorption by poultry litter and wood biochars in stormwater treatment, *Sci. Total Environ.*, 553, 596–606, <https://doi.org/10.1016/j.scitotenv.2016.02.129>, 2016.
- Tong, D., Zhuang, J., Lee, J., Buchanan, J., and Chen, X.: Concurrent transport and removal of nitrate, phosphate and pesticides in low-cost metal- and carbon-based materials, *Chemosphere*,

- 230, 84–91, <https://doi.org/10.1016/j.chemosphere.2019.05.056>, 2019.
- Uchimiya, M., Chang, S. C., and Klasson, K. T.: Screening biochars for heavy metal retention in soil: Role of oxygen functional groups, *J. Hazard. Mater.*, 190, 432–441, <https://doi.org/10.1016/j.jhazmat.2011.03.063>, 2011.
- US Patent and Trademark Office: Patent Application Full Text and Image Database, Pat. Appl. Full Text Image Database, available at: <https://www.uspto.gov/patents/search>, last access: 1 April 2021.
- Uttran, A., Loh, S. K., Kong, S. H., and Bachmann, R. T.: Adsorption of npk fertiliser and humic acid on palm kernel shell biochar, *J. Oil Palm Res.*, 30, 472–484, <https://doi.org/10.21894/jopr.2018.0029>, 2018.
- Verdouw, H., Van Echteld, C. J. A., and Dekkers, E. M. J.: Ammonia determination based on indophenol formation with sodium salicylate, *Water Res.*, 399–402, [https://doi.org/10.1016/0043-1354\(78\)90107-0](https://doi.org/10.1016/0043-1354(78)90107-0), 1978.
- Wang, B., Lehmann, J., Hanley, K., Hestrin, R., and Enders, A.: Adsorption and desorption of ammonium by maple wood biochar as a function of oxidation and pH, *Chemosphere*, 138, 120–126, <https://doi.org/10.1016/j.chemosphere.2015.05.062>, 2015a.
- Wang, B., Yang, D.-Y., and Li, F.-Y.: Removal of nitrate and phosphate by immobilized biochars prepared from reeds and hematite, *fresenius Environ. Bull.*, 26, 4825–4833, 2017.
- Wang, S., Kwak, J.-H., Islam, M. S., Naeth, M. A., Gamal El-Din, M., and Chang, S. X.: Biochar surface complexation and Ni(II), Cu(II), and Cd(II) adsorption in aqueous solutions depend on feedstock type, *Sci. Total Environ.*, 712, 136538, <https://doi.org/10.1016/j.scitotenv.2020.136538>, 2020.
- Wang, Y. Y., Lu, H. H., Liu, Y. X., and Yang, S. M.: Removal of phosphate from aqueous solution by SiO<sub>2</sub>-biochar nanocomposites prepared by pyrolysis of vermiculite treated algal biomass, *RSC Adv.*, 6, 83534–83546, <https://doi.org/10.1039/c6ra15532d>, 2016.
- Wang, Z., Guo, H., Shen, F., Yang, G., Zhang, Y., Zeng, Y., Wang, L., Xiao, H. and Deng, S.: Biochar produced from oak sawdust by Lanthanum (La)-involved pyrolysis for adsorption of ammonium (NH<sub>4</sub><sup>+</sup>), nitrate (NO<sub>3</sub><sup>-</sup>), and phosphate (PO<sub>4</sub><sup>3-</sup>), *Chemosphere*, 119, 646–653, <https://doi.org/10.1016/j.chemosphere.2014.07.084>, 2015b.
- Watanabe, F. S. and Olsen, S. R.: Test of an Ascorbic Acid Method for Determining Phosphorus in Water and NaHCO<sub>3</sub> Extracts from Soil, *Soil Sci. Soc. Am. J.*, 29, <https://doi.org/10.2136/sssaj1965.03615995002900060025x>, 1965.
- Web of Science: Core Collection Database, “Biochar,” available at: <http://apps.webofknowledge.com>, last access: 1 April 2021.
- Wickham, H.: *ggplot2: Elegant Graphics for Data Analysis*, Springer-Verlag New York, available at: <https://ggplot2.tidyverse.org> (last access: 1 May 2021), 2016.
- Wickham, H., Averick, M., Bryan, J., Chang, W., McGowan, L., François, R., Grolemund, G., Hayes, A., Henry, L., Hester, J., Kuhn, M., Pedersen, T., Miller, E., Bache, S., Müller, K., Ooms, J., Robinson, D., Seidel, D., Spinu, V., Takahashi, K., Vaughan, D., Wilke, C., Woo, K., and Yutani, H.: Welcome to the Tidyverse, *J. Open Source Softw.*, 4, 1686, <https://doi.org/10.21105/joss.01686>, 2019.
- Yang, H. I., Lou, K., Rajapaksha, A. U., Ok, Y. S., Anyia, A. O., and Chang, S. X.: Adsorption of ammonium in aqueous solutions by pine sawdust and wheat straw biochars, *Environ. Sci. Pollut. Res.*, 25, 25638–25647, <https://doi.org/10.1007/s11356-017-8551-2>, 2017.
- Yao, Y., Gao, B., Zhang, M., Inyang, M., and Zimmerman, A. R.: Effect of biochar amendment on sorption and leaching of nitrate, ammonium, and phosphate in a sandy soil, *Chemosphere*, 89, 1467–1471, <https://doi.org/10.1016/j.chemosphere.2012.06.002>, 2012.
- Yin, Q., Zhang, B., Wang, R., and Zhao, Z.: Phosphate and ammonium adsorption of sesame straw biochars produced at different pyrolysis temperatures, *Environ. Sci. Pollut. Res.*, 25, 4320–4329, <https://doi.org/10.1007/s11356-017-0778-4>, 2018.
- Yin, Q., Liu, M., and Ren, H.: Removal of Ammonium and Phosphate from Water by Mg-modified Biochar: Influence of Mg pretreatment and Pyrolysis Temperature, *Bioresources*, 14, 6203–6218, <https://doi.org/10.15376/biores.14.3.6203-6218>, 2019.
- Zeng, Z., Zhang, S., Li, T., Zhao, F., He, Z., Zhao, H., Yang, X., Wang, H., Zhao, J., and Rafiq, M. T.: Sorption of ammonium and phosphate from aqueous solution by biochar derived from phytoremediation plants, *J. Zhejiang Univ. B*, 14, 1152–1161, <https://doi.org/10.1631/jzus.B1300102>, 2013.
- Zhang, D., Yan, M., Niu, Y., Liu, X., van Zwieten, L., Chen, D., Bian, R., Cheng, K., Li, L., Joseph, S., Zheng, J., Zhang, X., Zheng, J., Crowley, D., Filley, T. R., and Pan, G.: Is current biochar research addressing global soil constraints for sustainable agriculture?, *Agr. Ecosyst. Environ.*, 226, 25–32, <https://doi.org/10.1016/j.agee.2016.04.010>, 2016.
- Zhang, H., Voroney, R. P., and Price, G. W.: Effects of Temperature and Activation on Biochar Chemical Properties and Their Impact on Ammonium, Nitrate, and Phosphate Sorption, *J. Environ. Qual.*, 46, 889–896, <https://doi.org/10.2134/jeq2017.02.0043>, 2017.
- Zhang, M., Song, G., Gelardi, D. L., Huang, L., Khan, E., Parikh, S. J., Ok, Y. S., Song, G., Gelardi, D. L., Huang, L., Khan, E., Parikh, S. J., and Ok, Y. S.: Evaluating biochar and its modifications for the removal of ammonium, nitrate, and phosphate in water, *Water Res.*, 186, 116303, <https://doi.org/10.1016/j.watres.2020.116303>, 2020.
- Zheng, H., Wang, Z., Deng, X., Zhao, J., Luo, Y., Novak, J., Herbert, S., and Xing, B.: Characteristics and nutrient values of biochars produced from giant reed at different temperatures, *Bioresour. Technol.*, 130, 463–471, <https://doi.org/10.1016/j.biortech.2012.12.044>, 2013.
- Zhou, L., Xu, D., Li, Y., Pan, Q., Wang, J., Xue, L., and Howard, A.: Phosphorus and Nitrogen Adsorption Capacities of Biochars Derived from Feedstocks at Different Pyrolysis Temperatures, *Water*, 11, 1559, <https://doi.org/10.3390/w11081559>, 2019.
- Zhu, Y., Murali, S., Stoller, M. D., Ganesh, K. J., Cai, W., Ferreira, P. J., Pirkle, A., Wallace, R. M., Cychosz, K. A., Thommes, M., Su, D., Stach, E. A., and Ruoff, R. S.: Carbon-based supercapacitors produced by activation of graphene, *Science*, 332, 1537–1541, <https://doi.org/10.1126/science.1200770>, 2011.